Ultrasonics Sonochemistry 83 (2022) 105949

Contents lists available at ScienceDirect

Ultrasonics Sonochemistry

journal homepage: www.elsevier.com/locate/ultson

# Effects of reservoir rock pore geometries and ultrasonic parameters on the removal of asphaltene deposition under ultrasonic waves

Ephraim Otumudia, Hossein Hamidi *, Prashant Jadhawar, Kejian Wu

*School of Engineering, King's College, University of Aberdeen, Aberdeen AB24 3UE, UK*

ARTICLE INFO

*Keywords:*
Ultrasonic waves
Formation damage
Asphaltene deposition
Glass micromodel
Pore geometries
Image analysis

ABSTRACT

Asphaltene deposition around the wellbore is a major cause of formation damage, especially in heavy oil reservoirs Ultrasonic stimulation, rather than chemical injection, is thought to be a more cost-effective and environmentally friendly means of removing asphaltene deposition. However, it seems to be unclear how crucial features like reservoir pore geometries and ultrasonic parameters affect this ultrasound treatment.

In this work, five two-dimensional glass micromodels with different pore geometries were designed to assess the impact of pore geometries on the ultrasonic removal of asphaltene deposition. Experiments were undertaken in an ultrasound bath at a set frequency (20 kHz) and adjustable powers (100–1000 W). Direct image analysis before, during and after sonication was used to assess the impact of pore geometry and a change in ultrasonic parameter on the removal of asphaltene deposition. The effectiveness of ultrasound treatment at various sonication periods were found to be reliant on the pore geometries of the individual micromodels. For micromodels with throat sizes 300 μm and pore shapes as circle, square and triangle, an increase in ultrasonic power from 400 to 1000 W resulted in an increase in the percentage of removed asphaltene deposition after 2 h from 12.6 to 14.7, 11.5 to 14.63, and 5.8 to 7.1 percent, respectively.

## 1. Introduction

Asphaltene is a complex crude oil fraction that is insoluble in light n-alkanes (like n-pentane or n-heptane) but soluble in aromatic solvents (like toluene or benzene) [1,2] . While asphaltene does not pose an issue while coexisting with in situ crude oil, various circumstances (such as a change in pressure, temperature, or the crude's composition) can disrupt the equilibrium of asphaltenes in the crude and cause them to precipitate [3]. The asphaltenes that have precipitated might cluster together (aggregation) and form bigger particles known as flocs [4,5] . Following that, the flocs may adhere to and build on reservoir rock surfaces, a process known as asphaltene deposition [6]. Asphaltene precipitation and deposition, particularly in heavy oil reservoirs, is a major cause of formation damage [7,8,9] . This phenomenon may present numerous problems in all stages of production from the petroleum reservoir by clogging, changing rock wettability from water-wet to oil-wet, and creating flow complexity particularly at the near wellbore region [10,1,11,3]. These problems have the potential to deter or completely stop the flow of oil, which will have a significant negative impact on oil recovery [1]. To treat or prevent asphaltene deposition, chemicals are frequently introduced into the formation [12,13], however, the method has some drawbacks, including environmental pollution, chemical compatibility with formation rock/fluid, chemical flammability issues, treatment longevity, chemical volume requirements, and human health concerns [14,15,16,17].

The use of ultrasonic waves to remediate asphaltene deposition is a non-destructive, environmentally friendly, and cost-effective technology that uses a simple ultrasonic downhole tool eliminates the need for specialized chemicals [18]. The method is gaining popularity in the petroleum industry [19], owing to its low energy consumption [18], high adaptability and zonal selectivity during treatment [20,21,22] .

Laboratory studies of ultrasonic treatment of formation damage are mainly conducted in one of two ways: in microfluidics/micromodels (capillary dominated flow) [23,19] or in a coreflooding experiment [24,25,20,26,27,28,29] . Glass micromodels have characteristics that are comparable to those of sandstone reservoir rock [6] and may be utilized to observe processes at the pore level under dynamic settings.

Salehzadeh et al. [19] investigated the effects of ultrasonic waves (frequency 20 kHz, power 40 W) on asphaltene flocculation and deposition using micromodels. In their experiment, they used a preventative

* Corresponding author.
*E-mail address:* hossein.hamidi@abdn.ac.uk (H. Hamidi).

https://doi.org/10.1016/j.ultsonch.2022.105949
Received 19 November 2021; Received in revised form 24 January 2022; Accepted 5 February 2022
Available online 8 February 2022

strategy and observed that ultrasound inhibited asphaltene deposition. Overexposure of samples to ultrasound worsened the damage, according to image analysis.

In another recent micromodel study, Rezaei Dehshibi et al. [23] studied the effects of ultrasonic waves on the removal asphaltene deposition. While asphaltene was precipitating in the micromodel, it was sonicated at a frequency of 30 kHz and a power of 100 W. Images were shown for which ultrasound inhibited asphaltene deposition, and it was believed that the mechanism underlying ultrasound's increased oil recovery was mostly vibrations.

Mousavi, S. M. R. et al. [30] compared the effects of ultrasonic treatment on heavy and extra heavy crude oil. Their research found that heavier crude oil has a longer optimal radiation period than lighter crude oil. Although the rate of viscosity changes is rapid for heavier oils, ultrasonic wave radiation has a larger impact on their viscosity. They concluded that ultrasonic waves could prevent macrostructure asphaltene flocs from forming in both heavier and lighter crude oils combined with n-alkenes. Other study found that ultrasonic waves can alter the kinetics of asphaltene flocculation in crude oils, lower the size of asphaltene aggregates, and increase rock permeability [31,32,33].

In the experiments involving ultrasound removal of both paraffin and scale precipitates, on core samples, it was found that permeabilities could be increased [20,24,25]. The frequency and power of the applied sound field have been discovered to affect the effectiveness of ultrasonic removal [20,25]. Increases in frequency and power (to 40 kHz and 1000 W, for example) can improve core treatment, although core damage can occur at frequencies higher than 40 kHz [20].

To aid in the removal of inorganic (NaCl and KCl) scales, ultrasonic treatment has been coupled with water injection [26,27]. Water injection combined with ultrasound resulted in greater permeability improvement than water injection alone. The results showed that when water injection and ultrasound were combined, the solubility of NaCl and KCl scales increased more than when ultrasound was used alone. For the low permeability cores, this treatment was more efficient [26].

Ultrasound has also been used, often in conjunction with other methods, to remove; formation damage caused by drilling and completion fluids [28], pore blockage by mud cake and mud particles [15] and fines [29], and partially hydrolyzed Polyacrylamide (PHPAM)-induced formation damage [34]. In general, it was found that ultrasound augmented the applied methods and increased pore permeability [28,29,34] . The ultrasound parameters (20 kHz, 1000 W and 100 mins sonication time) were effective in removing the formation damage [29,34] .

The above studies indicate that ultrasonic waves, along with various mechanisms, could remove or prevent formation damages and improve reservoir permeabilities. The effect of pore geometries on ultrasonic treatment in an asphaltene-induced formation damage, on the other hand, has not been investigated. There has not been a systematic investigation that compares the effects of different ultrasonic parameters on asphaltene-induced formation damage. Furthermore, the majority of micromodel research on the influence of ultrasound on asphaltene deposition have focused on qualitative analysis of asphaltene removal by ultrasonic waves, with just a few studies using micromodels for both qualitative and quantitative analyses.

In this paper, the effect of pore geometries and ultrasound parameters during ultrasound treatment of asphaltene deposition has been examined by using five 2D glass micromodels. The glass micromodels constructed in the laboratory represent the same design properties with differences in their pore shapes, throat sizes and coordination number. Many rocks contain flat, tabular, flaky, elongate or needle-like grains, thus the packing arrangement of these grains may result to pore spaces in form of a circle, square or triangle which is reflected in the micromodel design. The uniform structure of each micromodel ensures that parameters such as pore roughness and different aspect ratios have no effect on the process of asphaltene precipitation and deposition. And finally, the impact of different pore geometries and ultrasonic parameters on the ultrasound treatment of asphaltene deposition was assessed using qualitative and quantitative data gathered from the experiments.

## 2. Experimental set-up and procedure

### 2.1. Materials

Brine was used as the formation water to create connate water saturation. NaCl, $Na_2SO_4$, $MgCl_2$, $CaCl_2$ and KCl (supplied by Sigma Aldrich UK) were dissolve homogenously in de-ionized water to act as the synthetic brine. The composition of the salt components is shown in Table 1.

Pentane (supplied by Atom Scientific) was used to precipitate asphaltene from a synthetic oil. After asphaltene deposition, decane (supplied by Atom Scientific) was used as the oleic phase with a blue dye added to it to allow distinction of phases in the porous media. The viscosities of the fluids were measured using Anton Paar™ Viscometer at 20 °C. The kinematic viscosity of the brine and decane are 1.1439 and 1.3425 $mm^2/s$ respectively.

### 2.2. Experimental set-up and equipment

Five 2D glass micromodels with high contrast pattern (Fig. 1) were designed to mimic a typical sandstone reservoir [6,35] . The circular, square and triangular pore body shapes represent the difference in the pore geometries.

The physical and hydraulic properties of the micromodels are shown in Table 2. Porosity of the micromodel was determined using image analysis technique. First, micromodel was saturated with colored distilled water, and then it was photographed by use of a high-resolution digital camera. Porosity of the micromodel is simply the ratio of colored area of micromodel to the total area of the micromodel.

To create a suitable environment for the propagation of ultrasonic waves, an acrylic water bath is filled with water and a waterproofed immersible transducer is secured to the bottom of the bath. The micromodel is held 5 cm above the transducer surface, just under the surface of the water, by a custom micromodel holder. An ultrasonic generator with fixed frequency of 20 kHz, and adjustable powers of 100 – 1000 Watt was employed. A temperature probe is placed inside the acrylic water tank to record the temperature rise induced by ultrasound. A syringe pump (PHD Ultra, Harvard Apparatus) was used to inject and control the flow of fluids into the micromodel system. A dino-lite digital microscope (equipped with light source and connected to a computer) is used to record and capture the fluid flow processes and removal of asphaltene deposition in the micromodel system. A schematic of the experimental set-up is shown in Fig. 2.

### 2.3. Experimental procedure

#### 2.3.1. Fabrication of micromodel

The micromodel is created in a step-by-step procedure. To begin, CorelDraw is used to create the required pattern for the micromodel. The planned pattern is etched on a glass plate using laser methods to create the flow network channel on the glass while the glass is coated with anti-

**Table 1**
Brine Composition.

| Component | Salt Concentration (g/100 ml) |
|---|---|
| NaCl | 2.410 |
| $Na_2So_4$ | 0.290 |
| $MgCl_2$ | 0.540 |
| $CaCl_2$ | 0.118 |
| KCl | 0.088 |
| TDS | 3.446 |

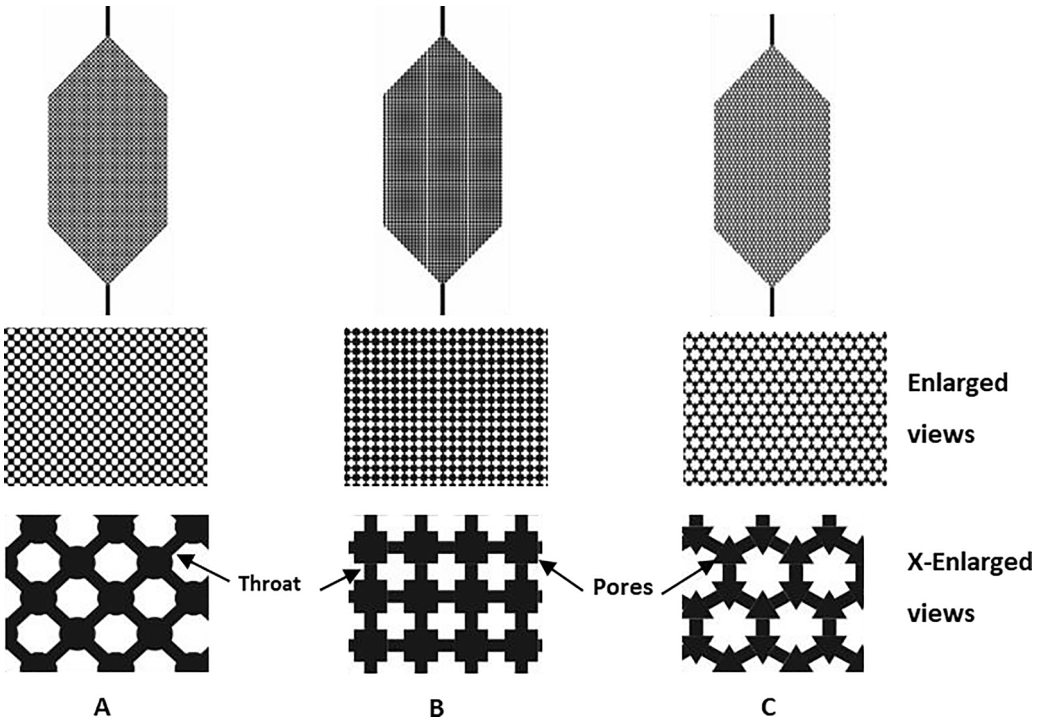


**Fig. 1.** Uniformly sized micromodel patterns used in the experiment A: circular pore-pattern (C-1 and C-2), B: square pore-pattern (S-1 and S-2), C: triangle pore-pattern (T).

**Table 2**
Design properties of 2D glass micromodels.

| Properties | Micromodels | | | | |
|---|---|---|---|---|---|
| | C-1 | C-2 | S-1 | S-2 | T |
| Pore shape | Circle | Circle | Square | Square | Triangle |
| Glass dimension (L*W), mm | 110 * 69 | | | | |
| Pattern dimension (L*W), mm | 87.5 * 42.3 | | | | |
| Etched depth, μm | 100 | | | | |
| Co-ordination number | 4 | 4 | 4 | 4 | 3 |
| Pore size, μm | 800 | | | | |
| Throat size, μm | 300 | 200 | 300 | 200 | 300 |
| Throat length, μm | 400 | | | | |
| Aspect Ratio | 2.67 | 4 | 2.67 | 4 | 2.67 |
| Porosity | 0.46 | 0.34 | 0.47 | 0.52 | 0.43 |

acid.

The etched pattern on the glass is then dug deeper using Hydrofluoric (HF) acid to a depth of roughly 100 μm in the next stage. The etched plate is next coated with a double layer of self-adhesive sandblast resist that is cut to expose the glass's inlet and exit channels. The glass is then sandblasted with saftigrit white aluminium oxide to create the micromodel's inlet and outlet channels.

The final step is to systematically bond the etched glass plate to another matching plain glass plate under high temperature to seal the micro channels. The glass is cleaned with Bohle premium glass cleaner and deionized water before being placed on the kiln shelf. The kiln is fired at 170 °C/hr to 695 °C, then the process is annealed at 250 °C/hr to 540 °C, and at 60 °C/hr to 400 °C to remove stress, before being turned off and allowed to cool overnight. When cool, a stainless steel (outer diameter 1/16 in.) is cut and sealed into the inlet and outlet port of the glass micromodel using epoxy resin.

### 2.3.2. *Asphaltene extraction and preparation of synthetic oil.*

Asphaltene was extracted from a North Sea crude oil sample using the ASTM D2007-80 method, a generally accepted standard for separating asphaltene from crude oil [36]. The asphaltene is extracted by adding n-pentane to the crude sample in the ratio of 40 to 1. The solution is then stirred and shaken for 4 h, before an equilibration resting period of two days, at ambient conditions, for asphaltene to precipitate. Afterwards, the solution is vacuum filtered to obtain asphaltene. The extracted asphaltene is washed with toluene and Soxhlet for two days to remove impurities. The obtained asphaltene-toluene solution is kept on a hot plate in the fume hood for toluene to evaporate. Then, asphaltene is dried and weighed to be ~ 4.5 g per 100 ml of crude. This weight determined the percentage of asphaltene for the preparation of synthetic oil.

Following, a synthetic oil is prepared by mixing a solution of 45% n-heptane and 55% toluene. The solution was then weighed, and the extracted asphaltene added to the main solution at a ratio of around 4.5% of its weight. [23,37] . Then the solutions were homogenized by mixing with a magnetic stirrer for 30 min. Because complex components and resins (found in crude oil) can inhibit asphaltene precipitation in the micromodel [38,39] , the synthetic oil is utilized instead of crude oil to precipitate asphaltene.

### 2.3.3. *Procedure for micromodel tests*

Before performing each experiment, the 2D glass micromodels were washed with toluene, acetone, and distilled water to remove impurities. Then, drained, vacuumed and dried in oven at 100 °C for 12 h to dry-off any fluids in the pores of the micromodel. The micromodel is placed in its holder and several pore volumes (PV) of brine solution are injected with the syringe pump to create initial water saturation. The micromodel is then is left undisturbed to equilibrate and for flow to become stable.

Following, synthetic oil is injected into the micromodel to displace the brine, until it can no longer be produced, and a connate water saturation is achieved. Flow is again allowed to stabilize before n-pentane is injected to induce asphaltene precipitation. The system was left overnight for asphaltene precipitants to flocculate and deposit on the walls of the micromodels. After asphaltene deposition, oil is injected without ultrasound until the asphaltene deposition level is not affected by the flow of the oil and the oil saturation in the system does not change

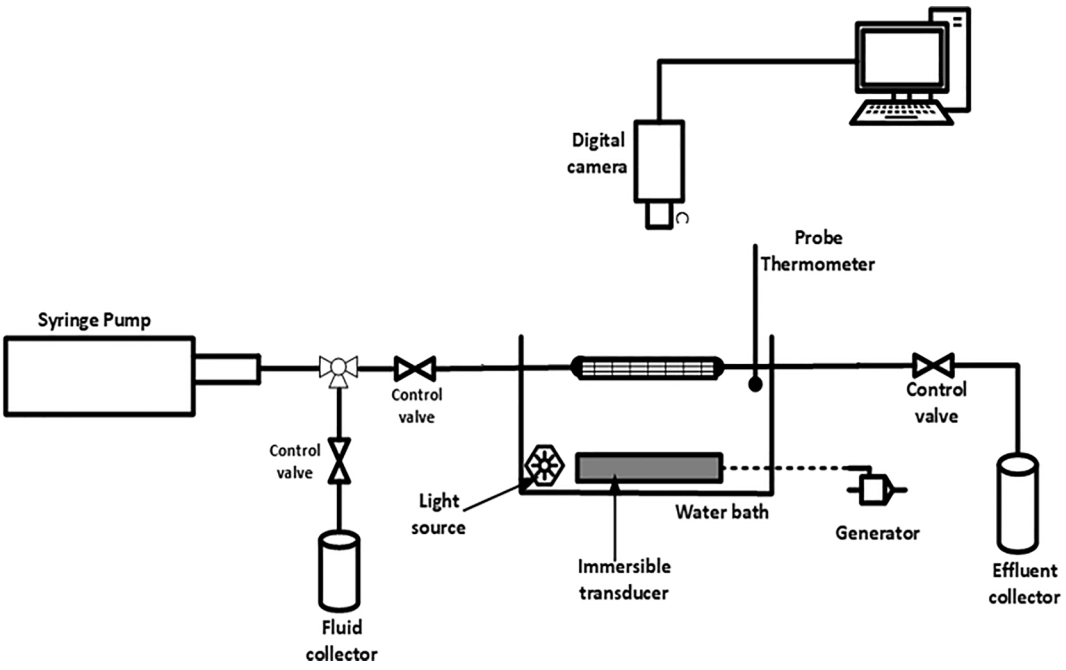


**Fig. 2.** Schematic of experiment setup.

with additional oil injection (that is, observations from image analysis shows no reduction in deposited asphaltenes or increase in oil saturation). Finally, ultrasound is applied to the micromodel with a simultaneous injection of oil to examine the impact of ultrasonic waves on the asphaltene deposition.

Macroscopic and microscopic tests were conducted to analyze this impact of ultrasonic waves on the whole system and at the pore level respectively. Sonication of the micromodels for all the experiment runs were limited to 2 h to reduce the length of each run in a day. The experimental conditions and the volumes of fluid injected were kept constant for all experiment runs. All fluids are injected at a constant rate of 0.6 ml/hour, to ensure a capillary dominated flow in the micromodel as well as a laminar flow. The capillary number, $N_{CA}$, for the simulated porous media was in the range of $N_{CA} = 10^{-7} - 10^{-6}$ which represents a typical flow in a sandstone reservoir. The micromodel experimental runs were carried out under ambient conditions. Repeated experiments showed an average error of not more than 5% and the general trend remained the same.

#### 2.3.4. Image analysis technique

Visual data acquisition was achieved by using high-resolution digital microscope (Dino-lite Edge AM7915MZT). Throughout the experiments, continuous video recording as well as images were captured to determine the effects of the ultrasound on the asphaltene deposits. The obtained images were segmented into three distinctive phases using ImageJ software. Finally, the segmented images were imported to MATLAB to obtain quantitative analysis of asphaltene deposition. MATLAB image processing gives the number of pixels of each of the phases and the number of pixels associated with the deposited asphaltenes were counted.

The percentage of removed asphaltene deposition to the total asphaltene deposition during the ultrasound treatment is calculated from the following equation:

$$\mathrm{AR}(\%) = \frac{A_{t0} - A_{tn}}{A_{t0}} \times 100$$

Where, $A_R$ is the removal rate of asphaltene deposition, $A_{t0}$ and $A_{tn}$ are the asphaltene deposits at time 0 and n respectively. Because of the horizontality of the micromodels and uniformity of the depth of the pores, it was assumed that the asphaltene depositions have the same thickness all through the micromodel. Subsequently, the area of the asphaltene deposition was utilized as a true representative of the amount of asphaltene deposition [40].

## 3. Results and discussion

### 3.1. Evidence of asphaltene deposition in glass micromodels

Asphaltene was first precipitated and allowed to deposit in each glass micromodel. Fig. 3 shows micromodel C-2 saturated with oil (blue), displaying several damages caused by asphaltene deposition (black) to the pores and throats of the micromodel. These damages could impede or redirect oil flow, resulting in pressure loss and low recovery during production. A pore scale visualization of asphaltene deposition before injecting oil in the micromodels are depicted in Fig. 4.

Fig. 4 (a and c) indicates that the asphaltene precipitation occurred in the pores, but some of the dispersed precipitate did not create deposition. It could be seen that the films of asphaltenes on the walls could change the wettability state (Fig. 4b). In the circle patterned micromodel C-2, asphaltenes deposited more on the pores than in throats (Fig. 4d, e, f) trapping the continual flow of pentane (Fig. 4e). Dead-end corners acted as retention sites for asphaltene deposition (Fig. 4 g-l) causing build up and blockage of the entire pores and throats (Fig. 4g, h, i). Deposited asphaltene plugged some throat areas reducing the paths of connectivity between the affected pores and the free flow of fluid (Fig. 4j, k).

### 3.2. Effect of different pore geometry on the removal of asphaltene deposition by ultrasound

#### 3.2.1. Macroscopic analysis of the whole micromodel under ultrasonic waves.

For the five micromodels of different pore geometries, Fig. 5 illustrates the percentage of asphaltene removed by ultrasonic treatment to the total asphaltene deposition. Ultrasound agitation fragmented the asphaltene deposits into tiny particles, increasing their solubility [41], however the rate of asphaltene removal were different for each micromodel. With a constant and continuous sweeping of the asphaltene

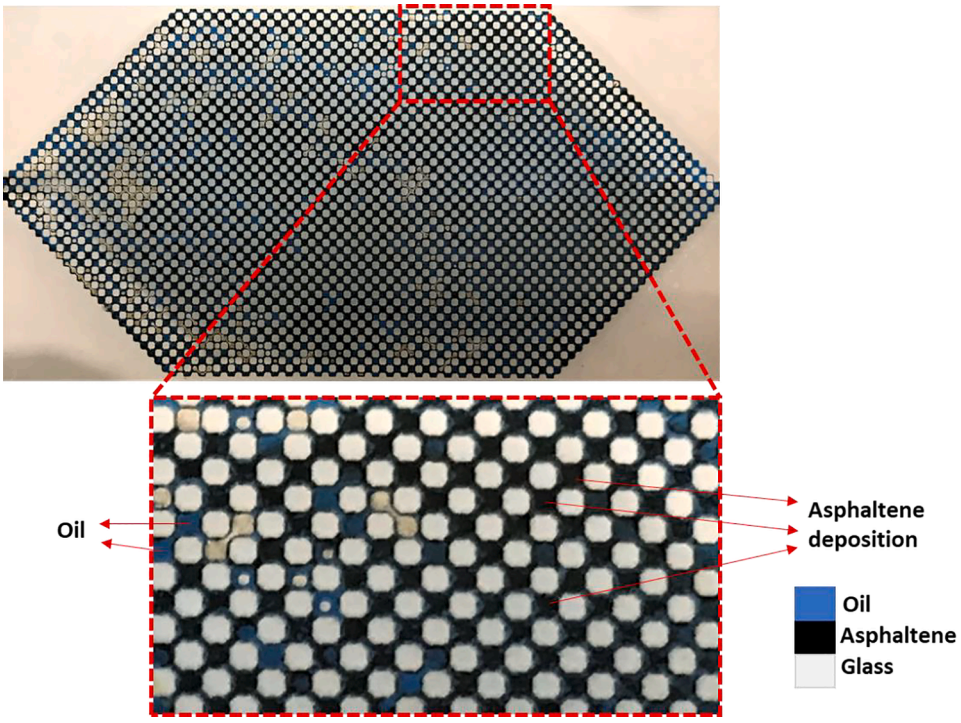


**Fig. 3.** Micromodel C-2 saturated with oil and showing various pores and throats damages due to asphaltene deposition.

deposition to 11.5% removal of total asphaltene deposition, ultrasonic treatment achieved around 75% of its 2 h performance for micromodel C-1 during the first 20 min. As sonication is continued after 20 mins, the impact of the ultrasound on the asphaltene deposition is reduced for micromodel C-1 and a slow increment in the percentage of removed asphaltene deposition is noted, reaching 15.6% removed deposition at 120 mins of sonication.

On the other hand, micromodel C-2, S-1, S-2 and T achieved about 2.0, 70, 12.2, and 80% of 2 h performance with steady dislodgement of asphaltene deposition that resulted in 0.3, 10.4, 1.3, and 6.1% removal of total asphaltene deposition respectively within their first 20 mins treatment. For the performance of ultrasound in Micromodel C-2, a slight improvement is seen from 20 mins to 40 mins and a jump to 60 mins and finally a slight suppression in the performance to an overall 13.9% removed asphaltene deposition. Micromodel S-1 followed a similar pattern from 20 mins to 60 mins but afterwards showed a bigger suppression in the performance to an overall 14.7% removed asphaltene deposition. Micromodel S-2 showed the weakest performance up to 80 mins of sonication compared to other micromodels, but subsequently experienced a jump in the percentage of removed asphaltene deposition to 10.6% total removal in 120 mins, whereas micromodel T showed a sluggish percent increment of removed asphaltene after the 20 mins of sonication. The only known differences in the micromodels that may have contributed to these inconsistencies in asphaltene removal are their geometries. For the different geometries (circular, square and triangle pore shapes), the trend of the plot for the percentage of removed asphaltene with respect to the sonication time were different. The geometries of the micromodel either enhanced or delayed the performance of the ultrasound treatment at different times. Fig. 6 gives a visualization of micromodel C-1 and C-2 during the application of ultrasound at 20 kHz and 1000 W.

Similar tests were conducted at that same conditions using the same ultrasonic frequency of 20 kHz, but different powers (400 and 600 W). The plots' patterns for the various applied powers revealed similar arguments about the effect of pore geometry on ultrasound treatment of asphaltene deposition. In all the tests, micromodel C-1 performed best in the removal of asphaltene deposits after 120 min of ultrasound treatment, followed by S-1, C-2, S-2, and T. Ultrasound required additional sonication time to remove all of the deposited asphaltenes in the micromodels, since the trends indicated that extended sonication might have an influence on asphaltene deposition.

### *3.2.2. Microscopic analysis of the micromodel pores and throats under ultrasonic waves*

Pores in each of the five micromodels were carefully picked from comparable sites and imaged at 230x magnification. Fig. 7 shows pore level images of asphaltene deposits during the application of ultrasound at 20 kHz and 1000 W.

In Fig. 7 (a), the imagery indicates substantial throat blockage on the left and on the right caused by asphaltene deposition which might obstruct oil flow and reduce the area filled by oil. Then, between 0 and 1.5 mins of sonication, ultrasound promoted fragmentation of a significant left-side throat blockage and some thinning of the right-side throat blockage, Fig. 7 (b). The fragmented asphaltene deposit is dispersed in the oil phase as the sonication time increases from 1.5 to 2.75 mins, and the right-side throat blockage is thinned further, Fig. 7 (c). The asphaltene deposition in the images, Fig. 7 (d to f), shows minimal change after 3.75 mins.

For micromodel C-2, the images of asphaltene deposits during ultrasonic treatment is shown in Fig. 8.

Fig. 8 (a) depicts a pore section of micromodel C-2 where asphaltene deposition has impacted the pore and throats. The images indicate minimal evidence of asphaltene deposition removal at the pore and throat areas, as seen in Fig. 8 (a to b). Then, as the sonication time is increased from 26.5 to 40 min, deposits on the right side of the pore are dislodged (Fig. 8 c). Some deposits from the dislodgement are expelled after 40 mins, as illustrated in Fig. 8 (d to e). After that, until the conclusion of the 120-mins sonication interval, the removal impact was negligible, as shown in Fig. 8 (e-f). The micromodel C-2 took longer than the micromodel C-1 to notice the influence of ultrasound on the deposited asphaltenes. The bond between the deposited asphaltenes and the throat walls might explain this. When the throat sizes get smaller, the bonds get harder, which slows up the breakdown and detachment of the asphaltene.

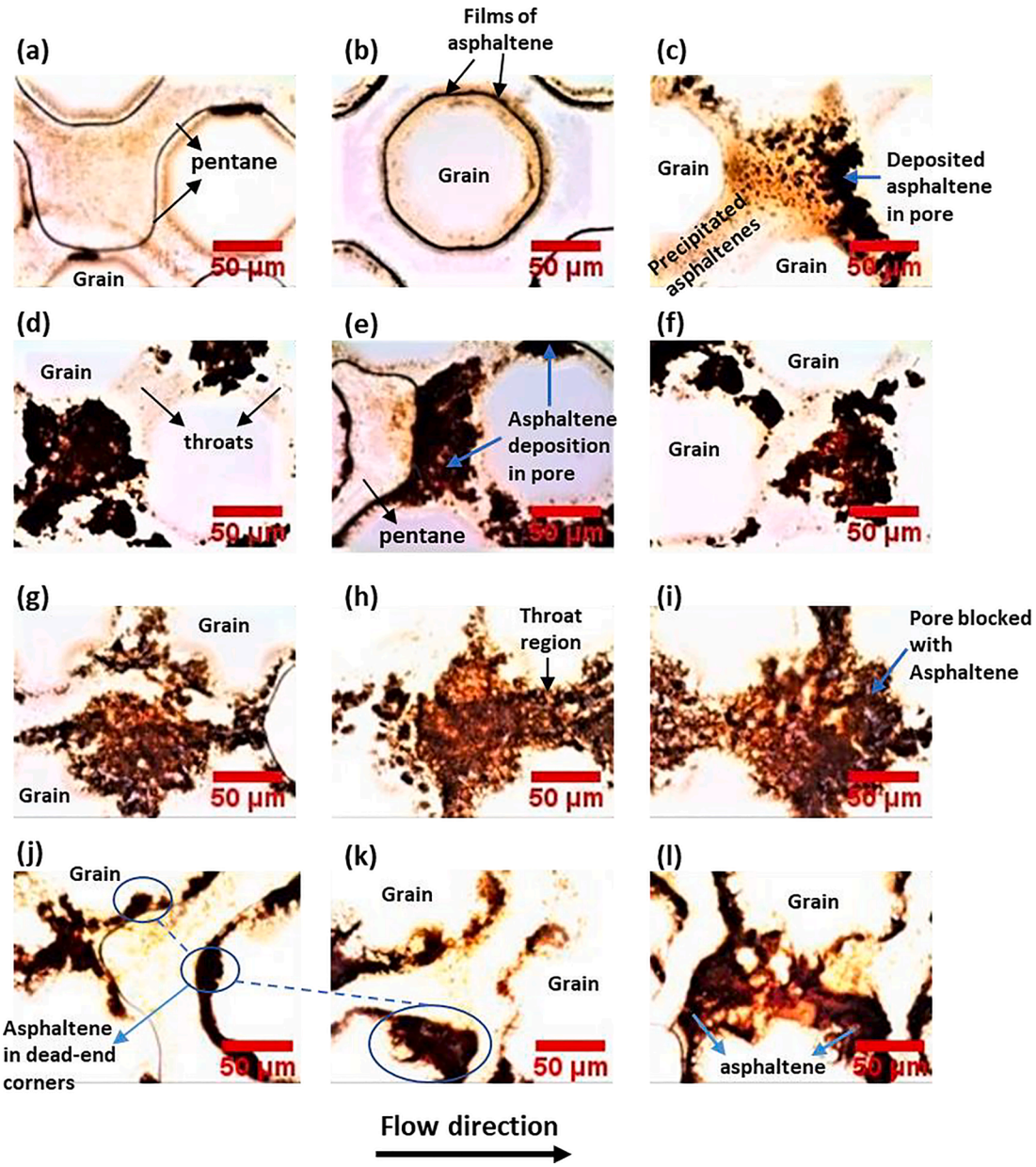


**Fig. 4.** Images of asphaltene deposition in homogeneous porous media at pore scale (a-c) micromodel C-1, (d-f) micromodel C-2, (d-f) micromodel S-1, (j-l) micromodel T.

The outcome of the microscopic examination on micromodel S-1 is illustrated. Fig. 9 shows the images during asphaltene removal by ultrasound at the pore scale.

After 7.5 mins of sonication, the blockage on the left-hand side of the pore eroded, and some removal was also evident on the right-hand side, Fig. 9 (c). Following that, the size of the asphaltene deposit on the right-hand side (of the right pore) decreases from 29 to 90 mins, as shown in Fig. 9 (d to e). Then it stays the same from 90 to 120 mins, Fig. 9 (f). More asphaltenes were retained in the pores than in throat, this may be explained by the Bernoulli's principle where pores becoming larger in comparison to the throat can cause lower fluid velocity [42] in the pores, which may have resulted to the increased asphaltene retention time in the pore regions than in throats.

Fig. 10 shows the images during asphaltene removal by ultrasound at the pore scale for micromodel S-2.

The images for micromodel S-2 reveal little dislodgement of asphaltene deposits from 0 to 78.5 mins, as seen in Fig. 10 (a to b). However, by 83 mins, some of the more sporadic deposits in the bottom left-hand pore had been removed, Fig. 10 (c). The large deposit on the right-hand side then begins to break down at 88 mins into the treatment, Fig. 10 (d) and is nearly completely removed by 120 mins into the treatment, Fig. 10 (f). There was no change after that till the completion of the 120 mins of sonication. Again, similar to micromodel C-2, it required a longer time for ultrasound to have a meaningful effect on the deposited asphaltene, which might be due to the enhanced bonding of asphaltene generated by smaller throat sizes.

Fig. 11 shows the images during asphaltene removal by ultrasound at the pore scale for micromodel T.

The imagery shows a little change to the asphaltene deposits, Fig. 11 (a to c), and a drop in the amount of deposited asphaltene from 27 to 77 mins, Fig. 11 (d to e). Here, the micromodel T presented less impact of ultrasound on the deposited asphaltenes. This may be due to the severity of the dead-end corners and the reduced connectivity between the pores (three coordination number). The sonication of the micromodels increases the velocity of fluid flow and more energy is exerted on the asphaltene depositions as fluid flows toward them which may contribute

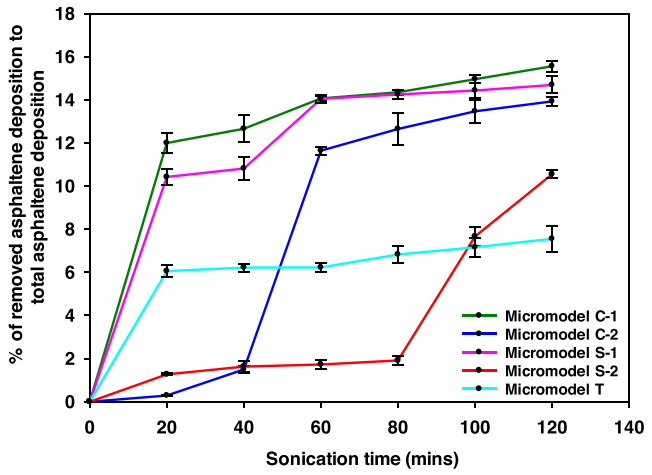


**Fig. 5.** Percentage of the removed asphaltene by ultrasound treatment (20 kHz, 1000 W) to the total amount of asphaltene deposition across the whole micromodel.

to the fragmentation of the asphaltene depositions. Ultrasonic waves, for all five micromodels, were shown in the presented images (Figs. 7 – 11) to fragment the deposited asphaltene and reduce blockage of pores and throats. Where blockage was reduced, there was an associated decrease in the amount of asphaltene deposit.

Fig. 12 shows the percentage of removed asphaltene deposition to total asphaltene deposition during ultrasound treatment for the different micromodels at their pore level.

In Fig. 12, micromodel C-1 shows a rapid incline in deposited asphaltene removal during the initial stage of treatment, where percentage removal reaches about 59% at 5 mins of sonication. After 5mins, there is little change to the percentage of removed asphaltene across the 2 h sonication time, as reflected in the leveling out on the line graph. In comparison with micromodel C-1, micromodel C-2 (which has a smaller throat size than C-1) showed a very small incline in the percentage of removed asphaltene from 0 to 26.5 mins (1.2% removal). Then, as sonication time increases from 26.5 to 40 mins, the percentage of removed asphaltene rises to 5.6%, but the most effective period of ultrasound treatment was observed from sonication time 40 to 61.5 mins, as reflected in the increase of percentage removal. For micromodel S-1, the trend of asphaltene removal shows the most effective period of ultrasound treatment to be 0–8.3 mins of sonication which saw about 41% increase in percentage of removed asphaltene, then further increase was seen in an unsteady manner but after 64 mins, percentage of removed asphaltene remains unchanged as shown in the levelling out of the graph. While for micromodel S-2, the most effective period of ultrasound treatment could not be seen until after 81.5 mins of sonication where the percentage of removed asphaltene soared continuously from 8.5% to 47% at 102 mins of sonication. Micromodel T had throat size 300 μm, but fewer coordination number (number of throats connecting the pores) than all other micromodels. Like micromodels C-1 and S-1, ultrasound aided an initial sharp rise in the percentage of asphaltene deposit removal in micromodel T, but the most effective period of treatment occurred between 32.75 and 52.75 mins with a jump in the percentage of removed asphaltene from 17.6 to 38.4%.

The larger throat size (300 μm) for circular, square and triangle micromodels showed greater initial asphaltene removal, than their small sized throat (200 μm) counterparts for which removal occurred at a later stage. For example, the micromodels with 300 μm throat sizes (C-1, S-1, and T) were shown to be more susceptible to the removal of asphaltene in the early stages of applied ultrasound. At 40 mins of sonication, the percentage of removed asphaltene reached 60.3%, 57.2% and 25.5% for micromodel C-1, S-1, and T respectively, while micromodel C-2 and S-2

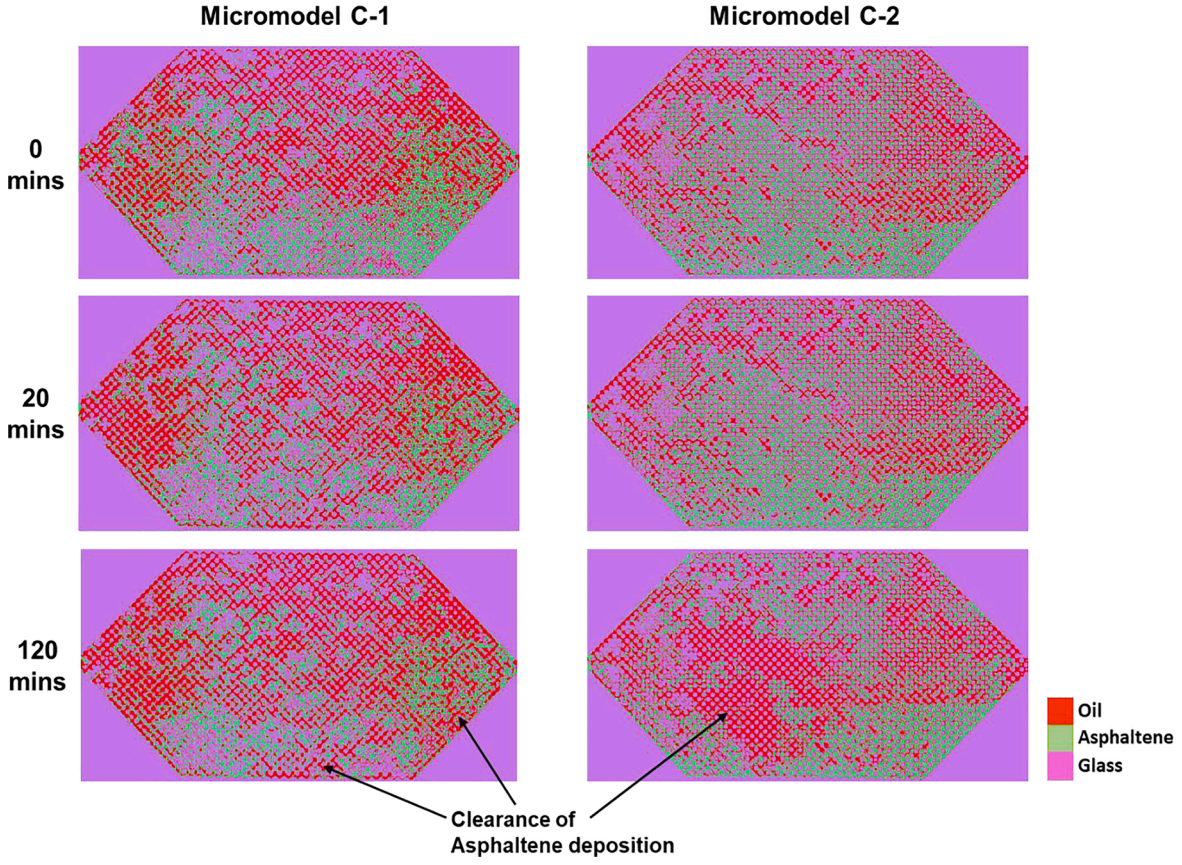


**Fig. 6.** Asphaltene removal across the whole micromodel (C-1 and C-2), by ultrasonic waves at frequency 20 kHz and power 1000 W.

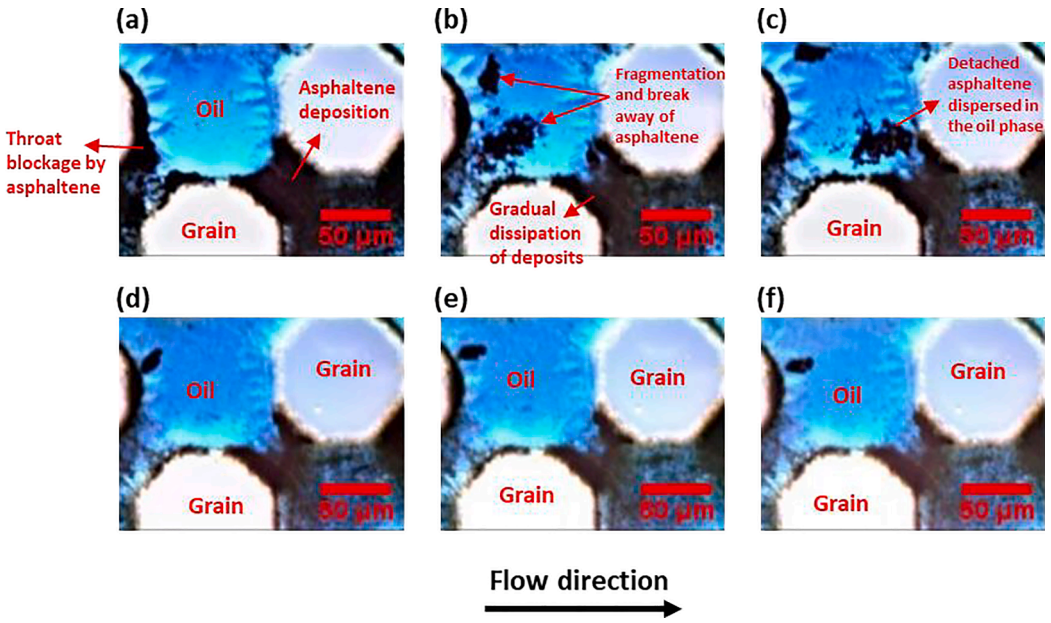


**Fig. 7.** Asphaltene removal, at pore scale, by ultrasonic waves (20 kHz, 1000 W) at different sonication times for circle patterned micromodel C-1 (a) 0 mins (b) 1.5 mins (c) 2.75 mins (d) 3.75 mins (e) 5.75 mins (f) 120 mins.

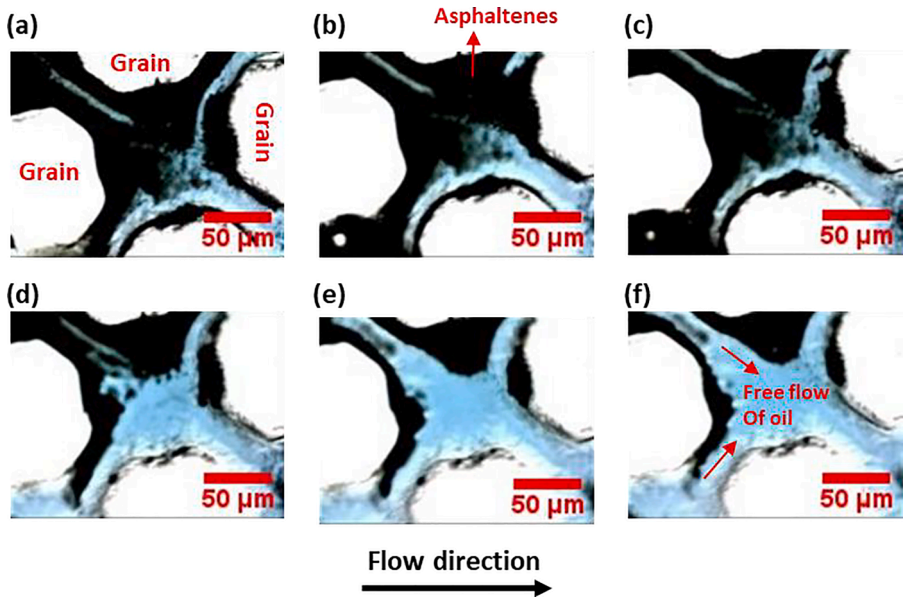


**Fig. 8.** Asphaltene removal, at pore scale by ultrasonic waves (20 kHz, 1000 W) at different sonication times for circle pattered micromodel C-2 (a) 0 mins (b) 26.5 mins (c) 40 mins (d) 52.5 mins (e) 61 mins (f) 120 mins.

yielded 6.1% and 7.4% respectively at 40 mins. Therefore, difference in throat sizes is found to affect performance of asphaltene deposition removal at the start of ultrasound treatment. The flattening of curves at a later stage of treatment in all micromodels requires the identification of an ideal sonication duration beyond which the influence of ultrasonic waves on deposited asphaltene becomes minimal. The investigated pores for all micromodels were found to have a high rate of asphaltene deposit removal by ultrasound, which did not match the total amount of asphaltene deposits removed from the whole micromodel. This is due to the fact that during oil flow, part of the asphaltene deposits that are removed from pores are retained in the pores that surround them and this can impact the results of the macroscopic analysis.

In general, these results show a distinction, for the different geometries of the pores, with regards to the effectiveness of ultrasound treatment of asphaltene deposition. Overall, ultrasound could breakdown and remove asphaltene deposition for all the tested micromodels. However, there was significant disparity in the sonication time required to loosen the asphaltene bond and initiate removal, and the effectiveness of continued treatment was dependent upon the geometries of the individual micromodels.

### 3.3. Ultrasound mechanism for observed trends of asphaltene removal

The application of ultrasound to a system can cause several known physical effects, namely; ultrasonic cavitation, fluid motion in the vicinity of cavitation bubbles (acoustic streaming and shockwaves), enhanced bulk liquid motion (quasi acoustic streaming), enhanced interparticle collisions and vibrational effects [43,41]. Since the

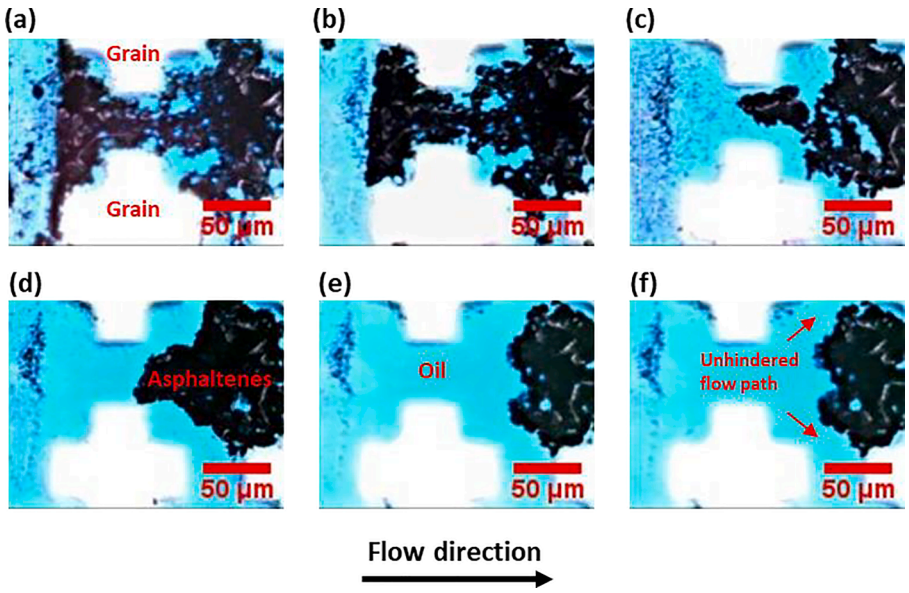


**Fig. 9.** Asphaltene removal, at pore scale, by ultrasonic waves (20 kHz, 1000 W) at different sonication times for square patterned micromodel S-1 (a) 0 mins (b) 5.25 mins (c) 7.5 mins (d) 29 mins (e) 90 mins (f) 120 mins.

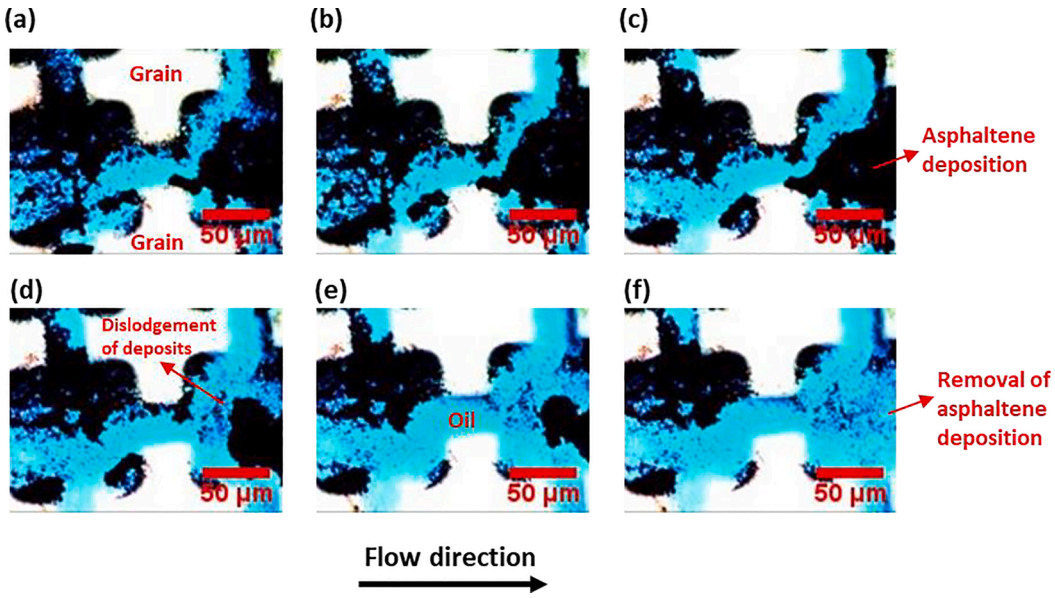


**Fig. 10.** Asphaltene removal, at pore scale, by ultrasonic waves (20 kHz, 1000 W) at different sonication times for square patterned micromodel S-2 (a) 0 mins (b) 78.5 mins (c) 83 mins (d) 88 mins (e) 101.5 mins (f) 120 mins.

asphaltene reduces volume available for cavitation and fluid flow, it is likely that the initial removal is caused by ultrasound vibration. The micromodel system, when subjected to vibration from the effect of ultrasonic wave could prompt relative movement of different molecules due to difference in their acceleration, resulting to breakage of asphaltene molecules [41]. The vibration can also cause the shear stress and acoustic pressure to vary intermittently. And for shear thinning fluids such as some heavy hydrocarbons, fluid viscosity decreases with an increase in shear stress. These effects together with a possible reduction in viscosity, may have contributed to the early removal of asphaltene deposition especially in micromodels C-1, S-1, and T (Fig. 12). It is envisaged that the vibrational effects of ultrasound to remove the deposits will be stronger for cases with minimal asphaltene bonding and where more asphaltene is present. This supports the data where enhanced deposit is observed in micromodels C-1 and S-1 at the pore scale. Thus, there is an initial strong removal period for C-1 and S-1 (Fig. 12).

The micromodels C-2 and S-2 that have smaller throat sizes (200 µm) than their counterparts, demonstrated some increases in removal after the initial (delayed) removal (Fig. 12). A smaller throat size may restrict fluid motion and thus allow any cavitation bubbles present to collapse with greater intensity [44]. Further, at this later stage the viscosity of the fluid may be reduced[45,46], thus, potentially increasing cavitation removal effects. Therefore, the removal of asphaltene for both small and large throat sizes may be due to a combination of vibration and cavitation effects.

As oil finds some path to flow within the blocked region, the vibrational force exerted on the asphaltene deposits may become less, resulting to the flattening of the curves in the later period of sonication for all micromodels. During this time, deposits around the edges of the

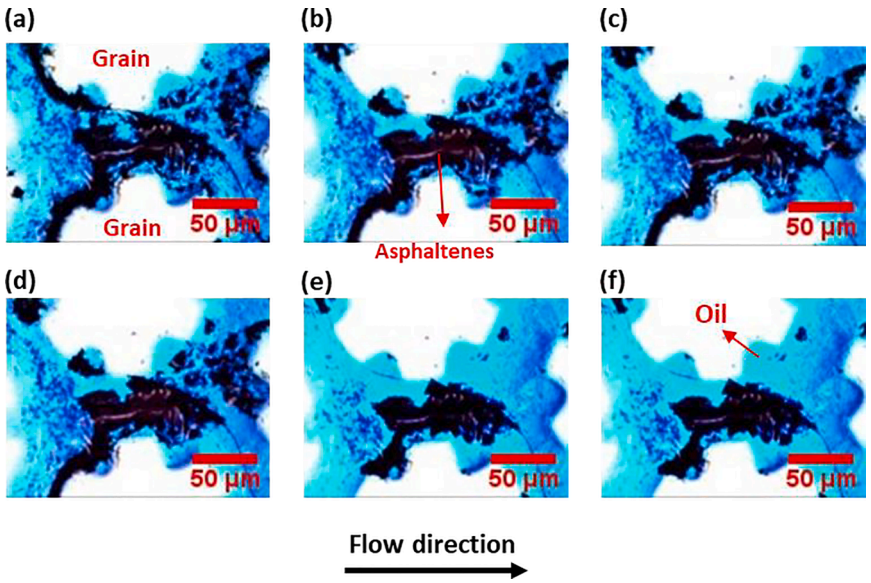


**Fig. 11.** Asphaltene removal, at pore scale, by ultrasonic waves (20 kHz, 1000 W) at different sonication times for triangle patterned micromodel T (a) 0 mins (b) 0.75 mins (c) 2mins (d) 27.75 mins (e) 77.75 mins (f) 120 mins.

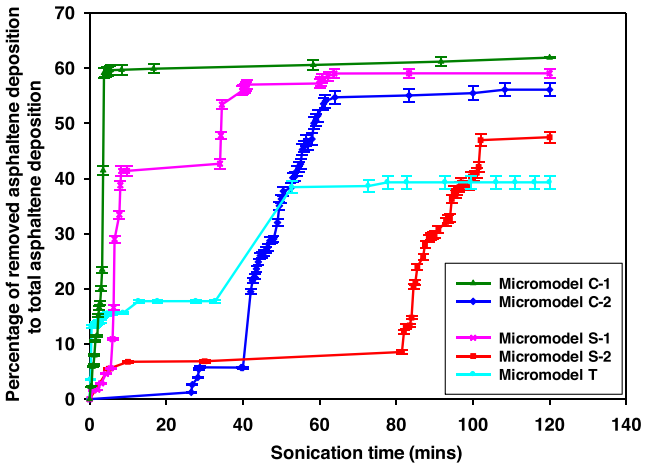


**Fig. 12.** Percentage removal of asphaltene deposit during ultrasound treatment (20 kHz, 1000 W) for different micromodel at their pore level.

pores take longer time to be combated, compared to regions that are completed blocked. This may imply a switch in mechanism from vibrational effects. Ultrasonic cavitation occurs when a high-intensity ultrasonic wave passes through a liquid, causing micron-sized gas bubbles to oscillate, grow, then rapidly implode, resulting in localized high temperatures and pressures within the collapsed spaces [47,48] . Therefore, where the deposited asphaltene has been removed, sufficient to provide enough liquid volume for cavitation to occur, this effect may cause further removal of deposit. It should be noted, however, that in more viscous fluids, such as heavy oil, the intensity of cavitation bubble collapse is reduced [49], but bubbles may become more stable in nature. As a result, the cavitation effect for this system may be minimal. Enhanced liquid motion, either of bulk solution (quasi acoustic streaming) or near cavitation bubbles (microstreaming)[50](with fragmented asphaltene) may also cause some removal of the remaining large deposits. However, for viscous fluids, fluid and particle motion is dampened by increased molecular bonding. Therefore, since the volume of available fluid, and the viscous nature of the fluid for cavitation and fluid flow effects is considerably reduced at the early treatment stage, then this may not explain the early asphaltene ultrasound removal. However, previous work has shown that the viscosity of oil can be reduced (from 68.2 to 63.5 cP) under ultrasound conditions (25 kHz, 500 W)[45] and viscosity reduction can cause a wettability change [23]. Therefore, at the later stage where asphaltene removal allows for more fluid volume in the micromodel and its viscosity is reduced, removal may be more due to these effects.

### 3.4. *Effects of ultrasonic parameters on asphaltene deposition*

The impact of ultrasonic parameters is investigated. It has been demonstrated that ultrasonic treatment is an effective approach for removing asphaltene deposition, and that the amount of asphaltene deposition removed may be maximized by increasing ultrasonic power and treatment duration.

#### 3.4.1. *Ultrasonic power*

By comparing Fig. 13 (a-e), it can be observed that as the ultrasound power increases, the increased radiation force resulted in an improved percentage of removed asphaltene deposition to total asphaltene deposition for the five micromodels examined, and the maximum percentage of removed asphaltene deposition is achieved when the ultrasound power is set at 1000 W.

While increasing the ultrasound power is positive for the removal of asphaltene, an excessive ultrasonic power could cause secondary emulsification which could be detrimental to oil recovery. Increasing the intensity of sound such that its energy is greater than that associated with the attractive forces between liquid molecules, can cause emulsification. The maximum critical ultrasonic power during the sonication was not observed in this experiment, which could be due to the low content of water in the system because oil was injected continuously.

Based on the analysis of the percentage of removed asphaltene deposition to total asphaltene deposition for the five micromodels (Fig. 13a-e), the percentage of removed asphaltene deposition can be maximized by increasing the ultrasonic power from 400 to 1000 W. This result is in agreement with the works of Wang et al. [20] where increases in ultrasonic power to 1000 W, improved core treatment by ultrasound on scale.

The relatively short range of ultrasonic waves, which normally does not exceed 1 m, is a common drawback in field applications. The depth of penetration is mostly determined by the applied frequency, the nature of the ultrasonic probe, and the density of the rock formation (M. [21].

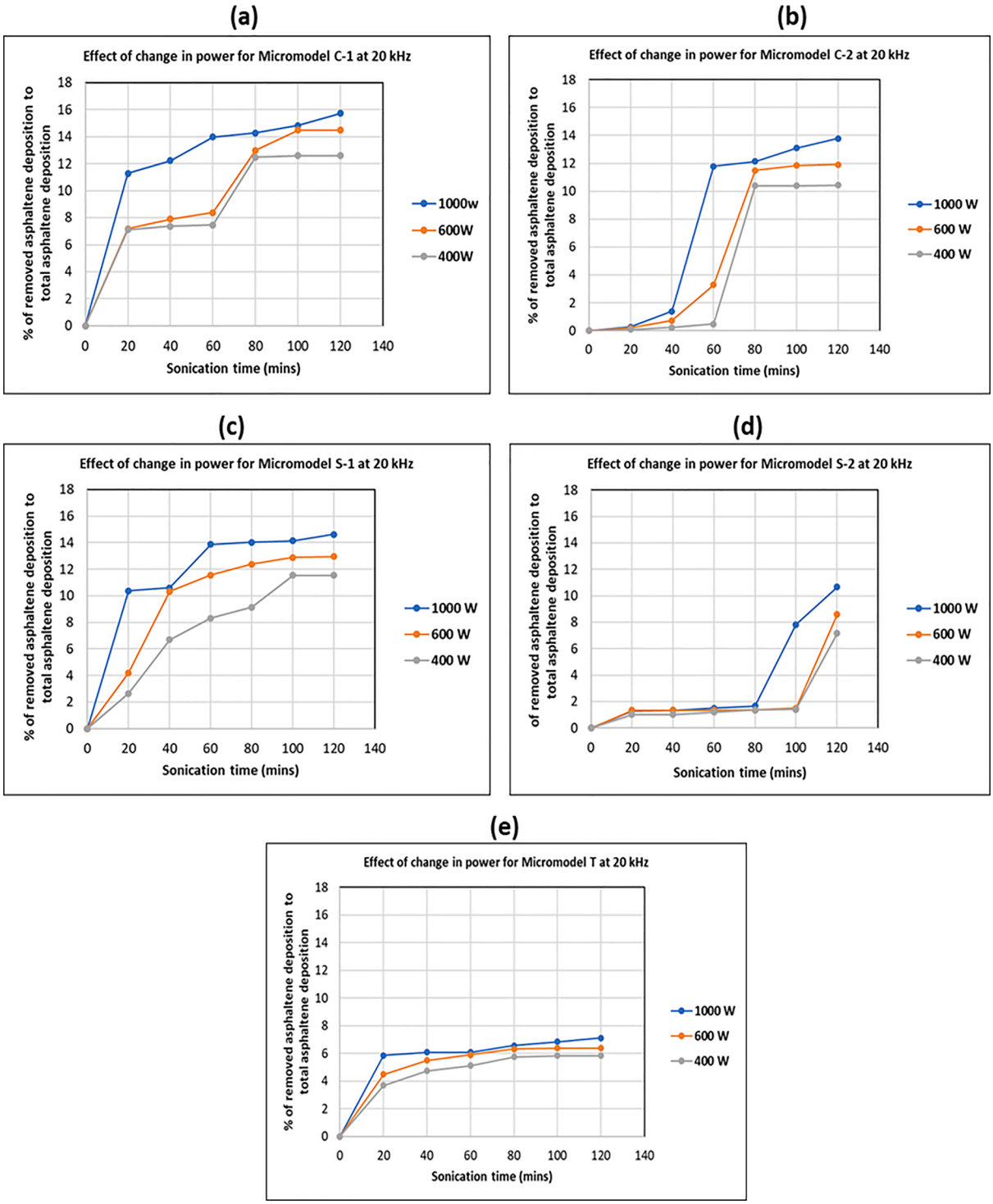


**Fig. 13.** Effect of a change in ultrasonic power during ultrasonic treatment of asphaltene deposition (a) micromodel C-1, (b) micromodel C-2), (c) micromodel S-1, (d) micromodel S-2, (e) micromodel T.

The lower the frequency, the deeper the penetration of the wave into the formation (M. [21,51] , while increasing the power will improve the cleaning effect. The 20 kHz frequency used in this study has been reported to penetrate up to 10 cm into the formation [22], and was adequate to remediate the near wellbore formation damage induced by paraffin precipitates [41].

### 3.4.2. *Ultrasonic sonication time*

For all micromodels, the percentage of removed asphaltene deposition to total asphaltene deposition increases as the sonication time increases (Fig. 13 a-e).

To reduce the overall time spent on each experiment per day, the total treatment time was set at 2 h. However, the findings imply that increasing the treatment time beyond 2 h will improve the effectiveness of ultrasonic treatment of asphaltene deposition and increase the percentage of removed asphaltene deposition. It is noted that the influence of ultrasound on the deposited asphaltene almost stabilizes after 100 mins for most micromodels, implying the need for determining an

optimal sonication time to reduce treatment costs.

It is worth noting that numerical simulations are a powerful tool for studying the behavior of systems and gaining additional insights, so creating a model for ultrasonic stimulation that accounts for fluid flow, precipitation, aggregation, and deposition of asphaltenes, as well as the interaction of ultrasonic effects in a porous media, is recommended.

## 4. Conclusions

In this study, different transparent porous micromodels, were designed, fabricated, and tested to quantitatively assess the impact of reservoir rock pore geometry and ultrasonic parameters on asphaltene deposition during ultrasonic stimulation. Based on the analysis, the following conclusions are drawn:

1) Pore geometries with dead-end corners are a favorable site for asphaltene retention and they create additional restrictions to the flow of fluid. The more severe the dead ends, the more susceptible it is for asphaltene to deposit, resulting to a different flow behavior and ultimately a lesser asphaltene removal by ultrasonic waves.
2) Reservoir geometries are critical to the success of ultrasound treatment of asphaltene deposition. Variation in the pore geometries, coordination number and throat sizes of the micromodels could enhance or delay the effectiveness of ultrasound treatment.
3) There is a period where ultrasound treatment of asphaltene deposition is most effective, and this period differs for different reservoir geometry.
4) With increased ultrasonic power (from 400 to 1000 W), asphaltene depositions decrease. Similarly, increasing the sonication duration, lowers asphaltene deposition.
5) Observations during ultrasound treatment shows that asphaltene deposition in smaller throats in terms of sizes, require longer sonication time to be removed, which may be due to the bond between asphaltenes and the walls.
6) To save treatment time, identification of an optimum sonication time beyond which, the effect of ultrasonic waves on the deposited asphaltene becomes immaterial is crucial.

### *CRediT authorship contribution statement*

**Ephraim Otumudia:** Conceptualization, Funding acquisition, Data curation, Formal analysis, Investigation, Methodology, Project administration, Validation, Visualization, Writing – original draft, Writing – review & editing. **Hossein Hamidi:** Conceptualization, Funding acquisition, Investigation, Methodology, Project administration, Resources, Supervision, Validation, Visualization, Writing – original draft, Writing – review & editing. **Prashant Jadhawar:** Conceptualization, Supervision, Writing – review & editing. **Kejian Wu:** Conceptualization, Supervision, Writing – review & editing.

### Declaration of Competing Interest

The authors declare that they have no known competing financial interests or personal relationships that could have appeared to influence the work reported in this paper.

### *Acknowledgement*

The authors are grateful to the Tertiary Education Trust Fund (TETFund) of Nigeria and University of Aberdeen UK, for providing the laboratory facilities required to complete this research. The contributions of Dr. Richard Wood and Gatiesh Marai, of the University of Aberdeen, are also appreciated.

### *Funding*

The research leading to these results received funding from Tertiary Education Trust Fund (TETFund) Nigeria (grant number RG14381-10), as a support for academic staff, training, and development.

Availability of data and material: Not Applicable.

Code Availability: Not applicable.

Ethics approval: Not applicable.

Consent to participate: Not applicable.

Consent for publication: Not applicable.

## References

[1] S. Fakher, M. Ahdaya, M. Elturki, A. Imqam, Critical review of asphaltene properties and factors impacting its stability in crude oil, J. Pet. Explor. Prod. Technol. 10 (3) (2020) 1183–1200, https://doi.org/10.1007/s13202-019-00811-5.
[2] Y.-J. Lin, P. He, M. Tavakkoli, N.T. Mathew, Y.Y. Fatt, J.C. Chai, A. Goharzadeh, F. M. Vargas, S.L. Biswal, Examining Asphaltene Solubility on Deposition in Model Porous Media, Langmuir 32 (34) (2016) 8729–8734, https://doi.org/10.1021/acs.langmuir.6b0237610.1021/acs.langmuir.6b02376.s001.
[3] K. Gharbi, K. Benyounes, M. Khodja, Removal and prevention of asphaltene deposition during oil production: A literature review, J. Petrol. Sci. Eng. 158 (2017) 351–360.
[4] Y.-J. Lin, P. He, M. Tavakkoli, N.T. Mathew, Y.Y. Fatt, J.C. Chai, A. Goharzadeh, F. M. Vargas, S.L. Biswal, Characterizing Asphaltene Deposition in the Presence of Chemical Dispersants in Porous Media Micromodels, Energy Fuels 31 (11) (2017) 11660–11668, https://doi.org/10.1021/acs.energyfuels.7b01827.
[5] S.S. Alian, A.A. Omar, A. Alta'ee, et al., Study of asphaltene precipitation induced formation damage during CO 2 injection for a Malaysian light oil, World Academy of Science, Engineering and Technology 78 (2011) 733–737.
[6] C.M. Seifried, Asphaltene Precipitation and Deposition from Crude Oil with CO2 and Hydrocarbons: Experimental Investigation and Numerical Simulation, Doctor of Philosophy in Chemical Engineering, Imperial College London Department of Chemical Engineering, 2016.
[7] A. Telmadarreie, J. Trivedi, Dynamic Behavior of Asphaltene Deposition and Distribution Pattern in Fractured Porous Media during Hydrocarbon Solvent Injection: Pore-Level Observations, Energy Fuels 31 (9) (2017) 9067–9079, https://doi.org/10.1021/acs.energyfuels.7b01347.
[8] ZhenBang Qi, A. Abedini, A. Sharbatian, Y. Pang, A. Guerrero, D. Sinton, Asphaltene Deposition during Bitumen Extraction with Natural Gas Condensate and Naphtha, Energy Fuels 32 (2) (2018) 1433–1439, https://doi.org/10.1021/acs.energyfuels.7b0349510.1021/acs.energyfuels.7b03495.s001.
[9] K. Keshmiri, H. Huang, N. Nazemifard, Microfluidic platform to evaluate asphaltene deposition during solvent-based extraction of bitumen, Fuel 239 (2019) 841–851.
[10] A. Hemmati-Sarapardeh, F. Ameli, B. Dabir, M. Ahmadi, A.H. Mohammadi, On the evaluation of asphaltene precipitation titration data: Modeling and data assessment, Fluid Phase Equilib. 415 (2016) 88–100.
[11] S.M. Mousavi, A. Ramazani, I. Najafi, S.M. Davachi, Effect of ultrasonic irradiation on rheological properties of asphaltenic crude oils, Pet. Sci. 9 (1) (2012) 82–88, https://doi.org/10.1007/s12182-012-0186-9.
[12] S. Alimohammadi, S. Zendehboudi, L. James, A comprehensive review of asphaltene deposition in petroleum reservoirs: Theory, challenges, and tips, Fuel 252 (2019) 753–791, https://doi.org/10.1016/j.fuel.2019.03.016.
[13] X. Xu, T. Bao, Research on the removal of near-well blockage caused by asphaltene deposition using sonochemical method, Ultrason Sonochem 64 (2020) 104918, https://doi.org/10.1016/j.ultsonch.2019.104918.
[14] J. Furgier, C. Lebecq, X. Degos, Formation Damage and the Importance of a Rigorous Diagnostic: a Case History in Nigeria Deep Water, SPE European Formation Damage Conference & Exhibition. (2013).
[15] B. Vakilinia, Experimental Investigation of Formation Damage Reduction: Mud Cake Removal and Mud Filtration Treatment using Ultrasonic Wave Radiation. SPE Annual Technical Conference and Exhibition, 2012.
[16] G. Hu, T. Liu, J. Hager, K. Hewage, R. Sadiq, Hazard assessment of hydraulic fracturing chemicals using an indexing method, Sci. Total Environ. 619-620 (2018) 281–290.
[17] V.H. Leong, H. Ben Mahmud, A preliminary screening and characterization of suitable acids for sandstone matrix acidizing technique: a comprehensive review, J. Pet. Explor. Prod. Technol. 9 (1) (2019) 753–778, https://doi.org/10.1007/s13202-018-0496-6.
[18] M.S. Mullakaev, V.O. Abramov, A.V. Abramova, Development of ultrasonic equipment and technology for well stimulation and enhanced oil recovery, J. Petrol. Sci. Eng. 125 (2015) 201–208.
[19] M. Salehzadeh, A. Akherati, F. Ameli, B. Dabir, Experimental study of ultrasonic radiation on growth kinetic of asphaltene aggregation and deposition, Can J Chem Eng 94 (11) (2016) 2202–2209.
[20] Z. Wang, J. Zeng, H. Song, F. Li, Research on ultrasonic excitation for the removal of drilling fluid plug, paraffin deposition plug, polymer plug and inorganic scale plug for near-well ultrasonic processing technology, Ultrason. Sonochem. 36 (2017) 162–167.
[21] M. Meribout, On Using Ultrasonic-assisted Enhanced Oil Recovery (EOR): Recent Practical Achievements and Future Prospects, IEEE Access 6 (2018) 51110–51118.

[22] M. Mohsin, M. Meribout, An extended model for ultrasonic-based enhanced oil recovery with experimental validation, Ultrason. Sonochem. 23 (2015) 413–423.
[23] R. Rezaei Dehshibi, A. Mohebbi, M. Riazi, M. Niakousari, Experimental investigation on the effect of ultrasonic waves on reducing asphaltene deposition and improving oil recovery under temperature control, Ultrason Sonochem 45 (2018) 204–212, https://doi.org/10.1016/j.ultsonch.2018.03.023.
[24] H. Xu, C. Pu, Removal of Near-wellbore Formation Damage by Ultrasonic Stimulation, Petrol Sci Technol 31 (6) (2013) 563–571, https://doi.org/10.1080/10916466.2011.586959.
[25] C. Pu, D. Shi, S. Zhao, H. Xu, H. Shen, Technology of removing near wellbore inorganic scale damage by high power ultrasonic treatment, Pet. Explor. Dev. 38 (2) (2011) 243–248.
[26] J. Taheri-Shakib, H. Naderi, Y. Salimidelshad, A. Teymouri, A. Shekarifard, Using ultrasonic as a new approach for elimination of inorganic scales (NaCl): an experimental study, J. Pet. Explor. Prod. Technol. 8 (2) (2018) 553–564, https://doi.org/10.1007/s13202-017-0369-4.
[27] J. Taheri-Shakib, H. Naderi, Y. Salimidelshad, E. Kazemzadeh, A. Shekarifard, Application of ultrasonic as a novel technology for removal of inorganic scales (KCl) in hydrocarbon reservoirs: An experimental approach, Ultrason. Sonochem. 40 (2018) 249–259.
[28] X. Shi, H. Xu, L. Yang, Removal of formation damage induced by drilling and completion fluids with combination of ultrasonic and chemical technology, J. Nat. Gas Sci. Eng. 37 (2017) 471–478.
[29] N. Khan, C. Pu, X.u. Li, Y. He, L. Zhang, C. Jing, Permeability recovery of damaged water sensitive core using ultrasonic waves, Ultrason. Sonochem. 38 (2017) 381–389.
[30] S.M.R. Mousavi, I. Najafi, M.H. Ghazanfari, et al., Comparison of Ultrasonic Wave Radiation Effects on Asphaltene Aggregation in Toluene-Pentane Mixture Between Heavy and Extra Heavy Crude Oils, J Energy Resour Technol 134 (2) (2012), 022001, https://doi.org/10.1115/1.4006435.
[31] I. Najafi, S.M.R. Mousavi, M.H. Ghazanfari, C. Ghotbi, A. Ramazani, R. Kharrat, M. Amani, Quantifying the Role of Ultrasonic Wave Radiation on Kinetics of Asphaltene Aggregation in a Toluene-Pentane Mixture, Petrol Sci Technol 29 (9) (2011) 966–974, https://doi.org/10.1080/10916460903394144.
[32] V.N. Kuryakov, Influence of ultrasonic treatment on kinetic of asphaltene aggregation in toluene/heptane mixture, J. Phys. Conf. Ser. 1942 (1) (2021) 012035, https://doi.org/10.1088/1742-6596/1942/1/012035.
[33] Najafi I, Amani M (2011) Asphaltene Flocculation Inhibition with Ultrasonic Wave Radiation: A Detailed Experimental Study of the Governing Mechanisms 2. 10.3968/ j.aped.1925543820110202.108.
[34] N. Khan, J. Pu, C. Pu, H. Xu, X. Gu, Z. Lei, F. Huang, M.A. Nasir, R. Ullah, Experimental and mechanism study: Partially hydrolyzed polyacrylamide gel degradation and deplugging via ultrasonic waves and chemical agents, Ultrason. Sonochem. 56 (2019) 350–360.
[35] M. Sharifipour, P. Pourafshary, A. Nakhaee, Study of the effect of clay swelling on the oil recovery factor in porous media using a glass micromodel, Appl. Clay Sci. 141 (2017) 125–131.
[36] J. Wang, J. Buckley, Standard Procedure for Separating Asphaltenes from Crude Oils, Accessed March/23 2020, http://baervan.nmt.edu/groups/petrophysics/media/pdf/prrc_02-02.pdf, 2020.
[37] H. Doryani, M.R. Malayeri, M. Riazi, Visualization of asphaltene precipitation and deposition in a uniformly patterned glass micromodel, Fuel 182 (2016) 613–622.
[38] M. Derakhshani-Molayousefi, M. McCullagh, Deterring Effect of Resins on the Aggregation of Asphaltenes in n-Heptane, Energy Fuels 34 (12) (2020) 16081–16088, https://doi.org/10.1021/acs.energyfuels.0c0306710.1021/acs.energyfuels.0c03067.s001.
[39] M.R. Yakubov, G.R. Abilova, K.O. Sinyashin, D.V. Milordov, E.G. Tazeeva, S. G. Yakubova, D.N. Borisov, P.I. Gryaznov, N.A. Mironov, Y.Y. Borisova, Inhibition of Asphaltene Precipitation by Resins with Various Contents of Vanadyl Porphyrins, Energy Fuels 30 (11) (2016) 8997–9002, https://doi.org/10.1021/acs.energyfuels.6b01503.
[40] N. Shahsavar, M. Riazi, M.R. Malayeri, Removal of asphaltene deposition in porous media using emulsified solvents - A visual study, J. Petrol. Sci. Eng. 191 (2020) 107207, https://doi.org/10.1016/j.petrol.2020.107207.
[41] H. Hamidi, A. Sharifi Haddad, E. Wisdom Otumudia, R. Rafati, E. Mohammadian, A. Azdarpour, W. Giles Pilcher, P. Wilhelm Fuehrmann, L. Ricardo Sosa, N. Cota, D. Cruz García, R.M. Ibrahim, M. Damiev, E. Tanujaya, Recent applications of ultrasonic waves in improved oil recovery: A review of techniques and results, Ultrasonics 110 (2021) 106288, https://doi.org/10.1016/j.ultras.2020.106288.
[42] D. Ni, in: Traffic Flow Theory, Elsevier, 2016, pp. 263–277, https://doi.org/10.1016/B978-0-12-804134-5.00019-2.
[43] K. Naderi, T. Babadagli, Pore-scale investigation of immiscible displacement process in porous media under high-frequency sound waves, J Fluid Mech 680 (2011) 336–360, https://doi.org/10.1017/jfm.2011.166.
[44] R.J. Wood, J. Lee, M.J. Bussemaker, Disparities between sonoluminescence, sonochemiluminescence and dosimetry with frequency variation under flow, Ultrason Sonochem 58 (2019) 104645, https://doi.org/10.1016/j.ultsonch.2019.104645.
[45] H. Hamidi, E. Mohammadian, R. Junin, R. Rafati, A. Azdarpour, M. Junid, R. M. Savory, The Effect of Ultrasonic Waves on Oil Viscosity, Petrol Sci Technol 32 (19) (2014) 2387–2395, https://doi.org/10.1080/10916466.2013.831873.
[46] X. Huang, C. Zhou, Q. Suo, L. Zhang, S. Wang, Experimental study on viscosity reduction for residual oil by ultrasonic, Ultrason Sonochem 41 (2018) 661–669, https://doi.org/10.1016/j.ultsonch.2017.09.021.
[47] M. Wan, S. Xu, T. Ding, H. Hu, R. Liu, C. Bai, S. Lu, Acoustic methods for cavitation mapping in biomedical applications, J. Phys. Conf. Ser. 656 (2015) 012007, https://doi.org/10.1088/1742-6596/656/1/012007.
[48] H. Nazari-Mahroo, K. Pasandideh, H.A. Navid, R. Sadighi-Bonabi, How important is the liquid bulk viscosity effect on the dynamics of a single cavitation bubble? Ultrason Sonochem 49 (2018) 47–52, https://doi.org/10.1016/j.ultsonch.2018.07.013.
[49] Y. Zhang, K.e. Chen, Y. You, W. Ren, Coalescence of two initially spherical bubbles: Dual effect of liquid viscosity, Int J Heat Fluid Flow 72 (2018) 61–72, https://doi.org/10.1016/j.ijheatfluidflow.2018.05.009.
[50] T. Leong, J. Collis, R. Manasseh, A. Ooi, A. Novell, A. Bouakaz, M. Ashokkumar, S. Kentish, The Role of Surfactant Headgroup, Chain Length, and Cavitation Microstreaming on the Growth of Bubbles by Rectified Diffusion, J Phys Chem C 115 (49) (2011) 24310–24316, https://doi.org/10.1021/jp208862p.
[51] X. Luo, H. Gong, Z. He, P. Zhang, L. He, Recent advances in applications of power ultrasound for petroleum industry, Ultrason Sonochem 70 (2021) 105337, https://doi.org/10.1016/j.ultsonch.2020.105337.